

Performance of a Micro-scale Radial-Flow Compressor Impeller made of Silicon Nitride

J.P. Johnston¹, S. Kang², T. Arima³, M. Matsunaga³, H. Tsuru³, and F.B. Prinz²

¹ Department of Mechanical Engineering
Stanford University
Stanford CA, 94305-3030, USA

Phone: +1-650-723-4024, E-mail: jpj@stanford.edu

² Mechanical Engineering, Stanford University
³ Wako Research Center, Honda R&D Co. Ltd., Saitama, Japan

ABSTRACT

A micro-scale, high-speed compressor impeller (12 mm diameter, 800,000 rpm) was built and tested for feasibility in regard to aerodynamic performance. The compressor might be applied in a fist-sized gas-turbine-generator. To survive high stresses at such high temperatures, the rotor was manufactured as a single turbine/compressor/shaft unit in silicon nitride. Tests were conducted in a cold-flow rig at reduced speed of 420,000 rpm. Results from a CFD code compared favorably to measured data at this speed. Extrapolation from test conditions to full design speed was accomplished by application of CFD applied at both speeds. The experiments confirm design rules regarding reduction of efficiency at low Reynolds number, and results with several blade-to-shroud clearances were obtained to illustrate the importance of this parameter on micro-scale compressor performance where blade-to-shroud clearances will be relatively large compared to conventional radial-flow compressors.

NOMENCLATURE

| | |
|------------|--|
| b_2 | Hub to shroud distance, diffuser width, 1 mm |
| b_{tip} | Blade span at impeller tip, 1 mm |
| C_p | Specific heat at constant pressure, 1005 (m ² /s ² -K) |
| k | Ratio of specific heats, $k = 1.4$ |
| Mg | Mass flow rate (g/s) |
| Mu | Work input coefficient, see Eq. (1) |
| N | Rotating speed (rpm) |
| P_c | Collection chamber pressure |
| P_2 | Static pressure at exit, (2) |
| PO_1 | Inlet total and static pressure |
| PO_2 | Total pressure at exit, (2) |
| R_2 | Radius of exit station, 6.9 mm |
| R_{tip} | Radius of the rotor at tip, 6 mm |
| TO_1 | Total temperature at inlet, (1) |
| TO_2 | Total temperature at exit, (2) |
| U_{tip} | Rotor tip speed: ωR_{tip} |
| Vt_2 | Tangential flow speed at (2) |
| Vt_{tip} | Tangential flow speed at tip |
| η | Adiabatic efficiency, see Eq. (2) |
| ρ_1 | density at inlet |
| ω | Rotating speed (rad/sec) |

INTRODUCTION

Very small gas turbines may, in the future, provide portable micro-sized power sources to be utilized in applications such as unmanned surveillance vehicles, autonomous robots and other light weight, mobile devices with power demand in the range from 10 to 100 Watts. It seems curious at first glance, but it has been shown that the power density of a gas-turbine engine is inversely proportional to its length scale; see: Kang (2002) and Epstein et al.

(2000). In this paper, the compressor for a fist-sized gas-turbine engine is the principal object of investigation.

Using conservative assumptions, analysis showed that a gas-turbine-generator based on a simple Brayton cycle with a cycle pressure ratio of 3:1 could produce the desired output (turbine shaft power of about 200 Watts) in a package of about 3 cm diameter by 9 cm long, excluding fuel tank and controls. The largest component is a reverse flow annular combustion chamber. The radial flow compressor and turbine rotors are much smaller, 12 mm diameter. They are mounted back-to-back on the shaft in an overhung configuration, ahead of the rear bearing. The generator, mounted between the front and rear bearings, is the second largest component of the package.

With rotors of this size, the shaft must spin at 800,000 rpm (500 m/s tip speed) to achieve the design pressure ratio of 3:1 using a radial flow compressor impeller with backward leaning blades. To withstand the high stresses at high temperature without the need for auxiliary cooling, a ceramic material, silicon nitride, was chosen for the rotors and shaft. Also, to attain the desired performance levels, the turbine and compressor had the fully three-dimensional geometry obtained in conventional turbomachines. This was achieved in the Stanford Rapid Prototyping Laboratory using the Mold SDM process to produce the intricate, three-dimensional rotors and shaft out of silicon nitride, as a single part.

The compressor rotor was designed with unshrouded blades, see Figure 1. The experimental configuration had 6 full blades and 6 partial blades (splitters) which are inclined backwards by 50 degrees at the tip. At the impeller tip, the radius, R_{tip} , is 6 mm, and the blade span, b_{tip} , is 1 mm. The blades are approximately 300 μ m thick, with a blunt trailing edge at the impeller tip. In the inducer region the blade thickness is slightly tapered and the blade leading edges are rounded, not tapered to a sharp edge, as would be the case if manufactured at larger scale. The hub-to-shroud depth at the impeller tip (diffuser inlet) equals the blade span at the tip, 1 mm. The blade-to-shroud clearance was originally designed to be 76 μ m, uniform from inducer inlet to the outlet at the impeller tip, R_{tip} .

At design point flow rate of 2.38 g/s, a work input coefficient (Vt_{tip}/U_{tip}) of about 0.7 was utilized so that the impeller would have enough pressure rise to produce a stage pressure ratio of 3.0 with an efficiency of 65 %. Loss estimates used in the preliminary design included low Reynolds number effects plus a tip clearance leakage loss of 4 percentage points in efficiency.

Downstream of the impeller, a vaned, radial-flow diffuser, proceeded by a short vaneless space, was designed for use in the actual engine. This diffuser should capture a portion of the impeller's exit dynamic pressure which represents about 21 % of the ideal total pressure rise or 40 % of the actual rise. To explore

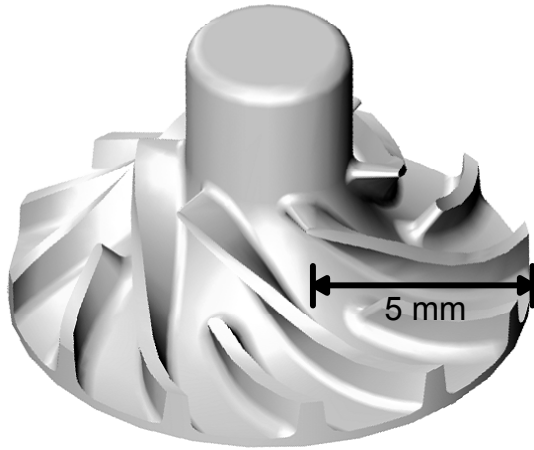


Figure 1 CAD model of the compressor impeller

the performance of the impeller alone, a vaneless diffuser (1 mm deep with a radius ratio of 2:1) ahead of an exit dump chamber was used for the current experiments and for the CFD (computational fluid dynamics) to be discussed below.

Bearings were a major issue. Air journal and thrust bearings were employed in the 4 mm diameter rotors of the 10 Watt micro gas turbine generator developed at the MIT Gas Turbine Laboratory (Epstein, et al., 2000). They were also used in the 10 mm rotors of the 100 Watt engine designed by IHI Co., Ltd, and Tohoku University (Isomura, et al., 2002). Modern developments in ball bearings for high speeds and small sizes, such as those used in air-turbines for dental drills, may also offer an option. For our experiments, ball bearings were employed for test speeds up to 420,000 rpm (260 m/s tip speed), close to the structural limit of the bearings and the speed limit of the cold-flow turbine in the facility.

This paper comments on the design and manufacturing of the turbine/compressor/shaft assembly, and evaluates compressor impeller performance by both experiment and from the results of CFD. In addition, because of the large blade-to-shroud clearances, some results on clearance effects were obtained.

Aerodynamic performance issues related to impeller size

Low Reynolds number, surface roughness, tip clearance, and minimum feature size are all important issues when one considers the design and performance of any miniaturized turbomachine. All four items can lead to reduced levels of performance, and thus require some discussion. Guidance is found in the literature (Casey, 1985) concerning Reynolds number and surface roughness effects. Tip clearance effects on the performance of centrifugal impellers is evaluated in Senoo and Ishida (1987). Also, useful information may be obtained from papers on an earlier micro compressor (4 mm diameter at 500 m/s tip speed) even though the radial flow path is unusual: flat and two-dimensional except for abrupt 90 degree turns between axial and radial flow (Epstein, 2000, and Jacobson, 1998).

Scaling of efficiency for shrouded, radial-flow compressor impellers, typical of narrow industrial compressor stages, was established by Casey (1985). He used a Reynolds number based on tip speed, U_{tip} ; blade height at the tip, b_{tip} ; and kinematic viscosity at impeller inlet, $1.5 \times 10^{-5} \text{ m}^2/\text{s}$ for air at room temperature and atmospheric pressure in the cases considered here. The method appears to work well when the flow through the impeller blade passages approximates turbulent flow in smooth or rough walled ducts.

For discussion, assume a large-scale, geometrically-similar, high Reynolds number impeller has a b_{tip} of about 1 inch, and compare it to this case where $b_{tip} = 1 \text{ mm}$; the scale ratio is 25:1. When Casey's scaling method is applied to both impellers with tip speeds of 500 m/s, a reduction in stage efficiency by 11 percentage

points is obtained for hydraulically smooth surfaces. If the surface roughness height is $1 \mu\text{m RMS}$, an additional 3 points is lost.

The Reynolds number for the micro-compressor impeller is 3.35×10^4 , which indicates that the flow in the impeller is turbulent, not laminar, and use of Casey's method is reasonable. However, if the size were reduced by another factor of 10, the losses would increase catastrophically. In that case, the flow would be laminar, and one may justifiably conclude that an impeller with a diameter of 1 to 2 mm may represent a lower limit, if efficiency is an important design criterion as it is here (Jacobson, 1998).

The current impeller does not have a rotating shroud like the impellers investigated by Casey (1985). There is no shroud cover over the blade tips, but the axial clearance to the stationary shroud is designed to be approximately 10 percent of the blade height, b_{tip} . Thus the losses predicted above are not going to be better than rough estimates. The friction losses may be smaller, but there will be an additional loss due to leakage over the blade tips, which should increase as the clearance increases. This added loss, which was assumed to be independent of scale, was originally estimated to be 4 points. Adding all losses together and assuming the design point efficiency of the micro compressor is 65 % says that a stage which is 25 times larger should have an efficiency of 83 %, a value in the expected range for this type of radial flow compressor operating at high Reynolds number.

Finally, the effects of minimum feature size need to be discussed. Here, the blade thickness was designed to be 0.3 mm (30 % of b_{tip}), and the blade leading edges were not sharp, as is the case in large high Mach number compressors of similar geometric shape. The thicker blades might reduce tip-clearance flows and losses at low Reynolds numbers. However, blunt leading edge effects should increase blockage downstream of leading edges (inducer region) and ultimately at the trailing edges of the blades. There is currently no way to accurately estimate the added losses and separate them from the flow distribution (thicker boundary layers) blockage effects due to low Reynolds numbers. Blockage is important in two ways: (i) It reduces the flow area compared to the available geometric area and thus limits the through flow. This effect may be accounted for in design by an increase in certain dimensions such as b_{tip} when a particular mass flow rate is required. (ii) Blocked area represents flow distortion which, compared to uniform flow, increases the mass-flow-average kinetic energy leaving the impeller. The downstream diffuser must cope with this non-uniformity as it reduces the kinetic energy and recovers it as static pressure rise. It is well known that increase of inlet blockage (flow distortion) leads to decrease in diffuser pressure recovery and consequently a loss in stage efficiency. In any case, the relatively large minimum feature size in the micro-scale compressor impeller is expected to have a negative influence on efficiency.

MICRO-SCALE CERAMIC COMPONENTS AND THEIR FABRICATION

Among the ceramic materials, silicon nitride can have exceptional high temperature properties as well as the low density (s.g. = 3.3, approximately). Its properties make silicon nitride a very attractive material for the components of mobile power sources. However, application of silicon nitride, in large- to mid-scale gas turbine engines, was hindered by the two major issues: reliability and difficulties in shaping parts, especially where joining parts is required.

This project was able to avoid the above issues by noticing the small length scale of the rotating components and the use of Mold SDM process in combination with gelcasting process.

Reliability of micro-scale ceramic components

Due to its brittleness, the strength of a ceramic specimen is decided by the biggest flaw in the critical load region. Since the size of the flaws typically follows a prescribed distribution, the strength of a ceramic specimen varies with the size of the part, for parts with the same geometry and process conditions.

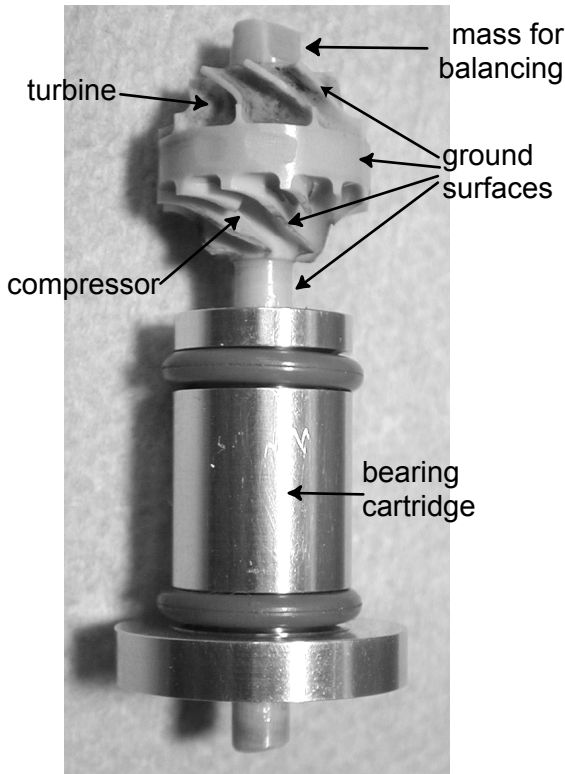


Figure 2 Rotor-group mounted in bearing cartridge.

Consequently, a probabilistic design concept is needed when structural ceramic parts are considered.

Application of Weibull statistics on the strength of ceramics shows that the survival probability of a ceramic specimen (P_s) is dependent on its volume as well as loading conditions and fabrication process (Wachtman, 1996). For highly dependable parts ($P_s \approx 1$), Kang (2002) shows that the probability of failure, which is defined as $P_f = 1 - P_s$, is proportional to the specimen's volume. Since the feature size of the rotor-group is about an order of magnitude smaller than for normal, ceramic turbines, significant reduction of failure probability is expected.

Mold SDM Process

In metal parts fabrication, complex but non-injection-moldable geometry can be achieved by joining with welding or other fastening methods. However, those approaches are not viable for complex ceramic parts and, thus, available geometry with conventional ceramic processes are limited.

The Mold SDM process is a derivative of the Shape Deposition Manufacturing (SDM) process (Cooper, et al., 1999). With Mold SDM one builds a mold for a complex part using the normal SDM process with combinations of two different classes of materials: mold material and support material. The support material forms the cavity of the final geometry inside of the mold material that forms the fugitive mold. The mold is completed by the removal of the support material. Application of the SDM process for mold fabrication allows the mold to have a complex

| Material | Strength (MPa) |
|------------------------------------|----------------|
| Si3N4 unpolished | 414 |
| Si3N4 polished | 950 |
| Si3N4 pressure sintering, polished | 983 |

Table 1 Strength values of Mold SDM silicon nitride (8.6Y₂O₃-3Al₂O₃-88.4Si₃N₄) measured in 4-point-bending at room temperature. The specimen size was 3 × 4 × 45 mm, (Stampfl et al., 2002).

internal geometry and a smooth surface finish of 1 μm RMS (Kang, 2002; Kang, et al., 2003).

Silicon nitride gelcast slurry is cast into the mold, and the slurry cures in the mold. Removal of the mold completes the green part. The subsequent steps in ceramic processing, which includes sintering, are the same as those used on other gelcast, ceramic parts.

Properties of Mold SDM silicon nitride

Ceramic parts reach their full strength (polished strength) after grinding and polishing. However, the geometry of a micro gas-turbine rotor-group only allows for limited grinding, just the cylindrical external surfaces (shaft, blade and rotor tips). Thus, the as-sintered strength, rather than polished strength is more meaningful in a discussion of the strength of Mold SDM silicon nitride parts, Table 1. The mean strength of Mold SDM silicon nitride is above 400 MPa as long as the mold surfaces are machined with the scallop height of 5 μm or lower (Stampfl et al., 2002). The rotor-group mold was fabricated with a scallop height of about 3 μm, so the failure strength of the rotor-group should exceed 400 Mpa at room temperature. Stresses in the rotor group at 800 krpm were obtained by finite-element stress analysis performed by M-Dot Aerospace, AZ. The predicted maximum stress of 290 MPa at the root of the compressor blade is less than the material strength.

VERIFICATION OF THE DESIGN BY CFD AND EXPERIMENTAL METHODS

The aerodynamic performance of a compressor in a rotor-group like the one shown in Figure 2 was ‘tested’ by two independent methods; (i) by direct measurements in a specially designed test facility, and (ii) by CFD analysis. The principal objective was to determine if the pressure ratio and efficiency at the design flow rate satisfied the requirements for ultimate, successful application in the gas turbine. Additional information on the effects of change of axial tip-clearance was also examined.

Test facility and procedures

The general goal was to verify the functionality of the compressor impeller alone at the highest possible rotor speed. No attempt was made to model the vaneed diffuser planned for the gas turbine itself. The shaft of the rotor-group fabricated with the Mold SDM process was mounted on two miniature ball bearings (3.175 mm ID) in an overhung position. The bearings were contained in a cartridge, Figure 2, supported on loaded rubber O-rings for vibration isolation and damping.

The rotor-group and bearing cartridge were placed in an axial traversing unit that was actuated by a micrometer as seen in Figure 3 (micrometer not shown). Thus, the rotor-group could be moved along the axis to vary the axial clearance between the blade tips and a fixed aluminum shroud wall. To assure failure-free operation in the primary test program (results in Figures 4-6), the axial gap at the rotor was set at 200 μm, larger than the design gap of 76 μm. This initial clearance was 20 % of b_2 , the blade span at rotor tip.

The shroud wall, on the right side in Figure 3, was machined from aluminum. It formed one wall of a 1 mm wide radial, vaneless diffuser. The opposite, left-side, wall of the diffuser ended abruptly at a radius of 12 mm in a 2 mm wide flow collection chamber. The left-side wall and collection chamber were formed as one part, integral with the turbine nozzle block. This complex part, which also included the turbine exit duct, was fabricated in Ciba TDT 205-3 polyurethane by the SDM method.

The turbine rotor was driven by high-speed flow from a radial cascade of converging nozzles (inclination to tangent of 20 degrees at outlet). Gas entered the nozzles from a common plenum itself fed by four axial pipes (one shown in the Figure 3). The turbine exhausted into the atmosphere through an axial diffusing duct. Compressed nitrogen at room temperature was the

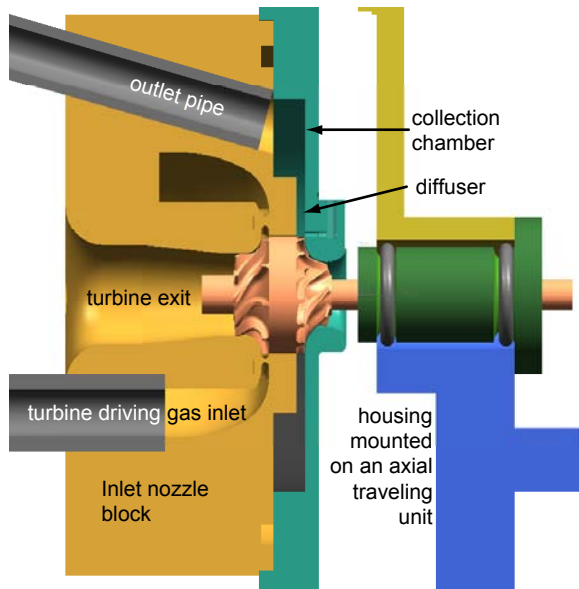


Figure 3 Cross section of inlet nozzle block, rotor-group, bearing cartridge and mounting unit.

driving gas giving the rotor a speed potential of about 500 krpm. Testing at the design speed of 800 krpm was not feasible.

The densification of the silicon nitride during the sintering process is accompanied by linear shrinkage (19±1% in this case). This shrinkage is accounted for in the design before the molds are made. To satisfy final accuracy requirements, certain surfaces such as turbine and compressor blade-shroud-contour profiles, the outer tip diameter and the shaft of the rotor were ground to fine tolerances. After grinding, the rotor was balanced while mounted on the bearings to a residual unbalance of 0.003 g-mm static, 0.003 g-mm dynamic at 1500 rpm. A combination of minute errors in rig machining and assembly combined with rotor vibrations when the rotor spins at high speed caused the speed limit of the rig to be 420 krpm to avoid short term mechanical failure.

Flow entered the compressor impeller through a smooth nozzle in the aluminum shroud wall. The four outlet pipes (only one shown above) from the collection chamber were connected to a common tube. This tube passed into a thermal flow meter and a flow control valve before the compressed air discharged to the atmosphere.

Performance of this compressor rotor was therefore determined at various speeds, up to 420 krpm, by measuring the pressures and temperatures at inlet and exit versus the mass flow rate. The small scale of the apparatus didn't permit detailed examination of the flow field leaving the impeller; only single point, average data at the exit (2) were possible. Details on the all measurements, instruments, and data analysis used for the performance evaluation are given by Kang et al. (2003). In addition to direct measurement of compressor mass flow rate, M_g , rotational speed, N , was measured by frequency analysis of light reflected from one end of the shaft. Control of N to an accuracy of ±1,200 rpm was provided by regulation of the nitrogen pressure entering the turbine.

P_{o1} , the impeller inlet total pressure is atmospheric, 101.4 kPa. The collection chamber pressure, P_c was measured, and pressures were measured at several spots inside the diffuser. A single tap was located at 6.185 mm, on the shroud wall almost at the impeller tip radius of 6.0 mm, but this proved unsuitable for performance evaluation. Finally, pressure taps were installed on opposite walls of the diffuser at a radius of 6.9 mm, slightly downstream of the impeller tip. Their average gave P_2 , the exit static pressure. The exit total pressure, P_{o2} , was computed by the method shown in Kang, et al., 2003. This method requires data on

the total temperatures, T_{o1} and T_{o2} , in addition to Mg, N, P_{o1} , and P_{o2} .

Temperature was measured at inlet (1) and exit (2). T_{o1} , was obtained from a thermocouple placed near the inlet bell. It ranged from 289 to 296 K. Downstream of the exit station, bare thermocouple wires (0.127 mm dia., type K) were inserted through a hole in the aluminum shroud-wall, bent over in the radial direction with the junction set as close to the impeller as possible. Between the hole and the junction, the bare wires comprised a 3 mm long stem. This was necessary to avoid substantial conduction cooling of the junction by the shroud-wall, which was always at about room temperature. Special consideration was needed to obtain the stagnation temperature, T_{o2} , because of the high speed of the flow (order 100 m/s) over the thermocouple probe. The raw readings were corrected by use of an aerodynamic recovery factor of 0.66 based on the tangential speed in the location of the junction.

Temperature rise gives adiabatic work input, $C_p (T_{o2} - T_{o1})$. Which, when combined with Euler's turbine equation for the same result provides the work-input coefficient (upon division by tip-speed squared):

$$Mu = V_{tip}/U_{tip} = C_p (T_{o2} - T_{o1})/U_{tip}^2 \quad (1)$$

The pressure ratio (P_{o2}/P_{o1}) and the adiabatic efficiency, η , require the estimation of the exit stagnation pressure, P_{o2} . It was assumed that air is a simple perfect gas, the velocity profiles at exit are uniform, and the flow fills the exit (no flow blockage).

The adiabatic efficiency is given by:

$$\eta = T_{o1} \{ (P_{o2}/P_{o1})^{(k-1)/k} - 1 \} / (T_{o2} - T_{o1}) \quad (2)$$

Finally, the errors in the data and the results derived from the data were obtained by a standard method for estimating uncertainty in single-sample experiments, Table 2.

Outline of the CFD method

The CFD code used here is based on a compressible-flow, Reynolds-averaged, Navier-Stokes method developed for computation of turbine and compressor rotor flows, Arima, et al. (1999). A low-Reynolds-number k-ε turbulence model is incorporated, and the code uses structured, non-orthogonal, body-fitted meshes. For this case, one blade-to-blade passage was divided by the splitter into two primary *streamtubes*, which extended from inlet to just downstream of the exit in the vaneless space. The mesh sizes for the *streamtubes* were 196×94×49. A uniform clearance gap of 100 μm (10 % of b_2) was incorporated in geometry used for the results shown in Figures 4-6. Computations were carried out at 800,000 rpm, the design-condition, and at the test condition of 420,000 rpm, so that direct comparison to the

| Quantity | Units | Uncertainty (20:1 odds) |
|---------------------|--------------|--------------------------------|
| Rotor speed | rpm | ±1200 |
| Mass flow | g/s | ±0.05 |
| Pressure | kPa | ±6 |
| Temperature | °C | ±1 |
| P_{o2}/P_{o1} | -- | ±0.04 (at 420,000 rpm) |
| $(T_{o2} - T_{o1})$ | °C | ±1.5 (") |
| Work input, Mu | -- | ±0.03 (") |
| Efficiency, η | -- | ±0.015 (") |

Table 2 Experimental Uncertainty according to Kline and McClintock (1953).

experimental results would be possible. Values of the properties at the exit (2) were obtained by mass flow averaging the detailed results at radius R_2 in the vaneless diffuser.

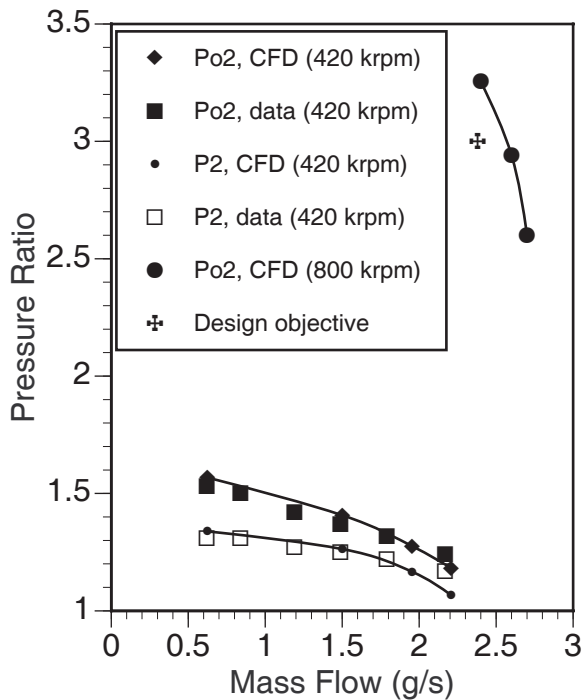


Figure 4 Pressure ratios, at test and design rotor speeds. Pressure ratios based on either total pressure, P_{o2} , or static pressure, P_2 , at impeller exit.

EXPERIMENTAL AND CFD RESULTS

Pressure ratios and temperature differences first were examined for consistency, and to check that the experimental results were reasonable. Figure 4 shows both data and CFD results for two pressure ratios, the static pressure ratio, P_2/P_{o1} , and the stagnation pressure ratio, P_{o2}/P_{o1} , plotted versus the mass flow rate at 420 krpm. The pressure ratio at 800 krpm, the design condition, is also shown together with a single point for the original design objective. The scatter in the data points is less than estimates of the uncertainty in the pressure ratio data. The best comparison between experiment and CFD is the check using static pressure ratio, P_2/P_{o1} , because these represent 'raw' data with no need to use temperature data too. Except for the point at highest flow rate, all results are in fairly close agreement. However, it can't be concluded that either result is more accurate than the other because of fundamental differences between the two methods. For example, surface roughness effects, accuracy of blade angle settings at leading edges, axial tip clearances (see below) may all lead to small differences between experimental and CFD results.

Measured temperatures, but not pressures, are needed in the calculation of the work input coefficient, Mu . Figure 5 shows some results where the negative slope of the constant speed curves is typical of radial flow impellers with backward leaning blades. At 420 krpm, the test data are in agreement with the CFD results. Preliminary experiments with the exit thermocouple placed in the collection chamber gave lower Mu values, which resulted in unreasonably high efficiencies. This was thought to be the result of significant heat losses to the walls of the vaneless diffuser. Heat transfer effects can be a significant issue in micro-scale devices (Epstein, et al., 2000), and this is the reason that the exit thermocouple was placed as close to the impeller tip as possible.

Scaling of the pressure ratio results between different rotor speeds, in the case of slightly compressible flow is accomplished by use of a dimensionless parameter, the *flow coefficient*, which in our case looks like, $Mg/(\rho_1 R_{tip}^3 \omega)$. Here, the inlet density and impeller tip radius are the same so a line of similarity which scales the mass flow rate, Mg , through the design point is: $Mg = Mg_{dp} [\omega / \omega_{dp}]$. The original design point at 800 krpm had a pressure ratio of 3 and mass flow rate of 2.38 g/s. The scaling gives a mass flow

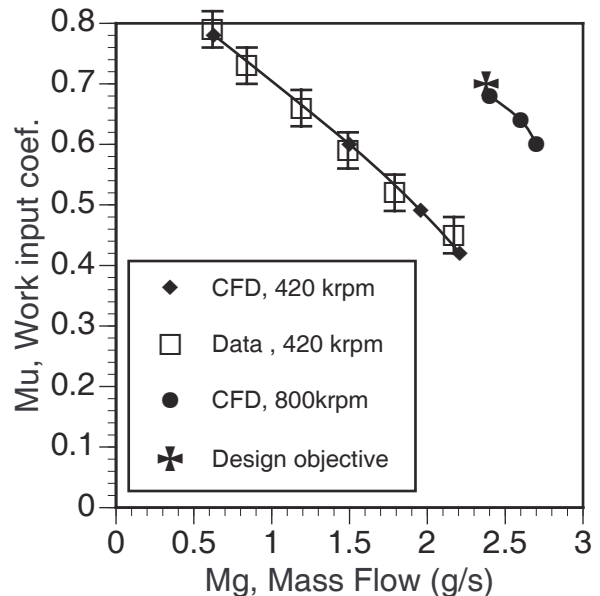


Figure 5 Work input coefficients, at test and design rotor speeds.

of 1.25 g/s as the approximate design point when operating at 420 krpm. Using the data in Figures 4 and 5 implies that $Mu = 0.65$ and $P_{o2}/P_{o1} = 1.42$ at 420 krpm.

The shape of the curves at design speed is somewhat different from their shapes at 420 krpm. This is because compressibility is more important at 800 krpm, and simple similarity scaling cannot be exact. In particular, at the highest flow rate, local choking effects near the blade leading edges will cause a sharper downturn in the pressure ratio and efficiency, and, at flows less than the lowest in the figures, an instability, surge, will be much more important at higher impeller speeds. This paper addresses neither choke or surge.

The adiabatic efficiencies for 800 krpm and 420 krpm are compared in Figure 6. The measured efficiency is about 0.04 points lower than the CFD results around the design-point-similarity (DPS) flow rate of 1.25 g/s. At high flow rate compared to DPS flow, the CFD result drops to lower efficiency values than is suggested by the data.

Two other sets of data were used in the calculation of the efficiency at 420 krpm. One is based on the measured static pressure ratio, (P_2/P_{o1}), at the exit station, and the other on the pressure ratio is based on the downstream collection chamber pressure, (P_c/P_{o1}). Both illustrate the need for an effective diffuser design. Figure 6 shows adiabatic efficiencies that are 0.24 and 0.18 points lower than the total-to-total (P_{o2}/P_{o1}) efficiency. To reduce the significant downstream diffuser losses implied here, a very effective vanned diffuser design will be required for the actual compressor stage, not a simple vaneless space, see Jacobson (1998).

The efficiency was measured for a range of lower speeds, down to 180 krpm. It was found, in the region of the DPS, that efficiency decreased as speed increased up to 420 krpm. When the CFD results are also included, a nearly linear decrease in design point efficiency is noted all the way to 800 krpm. An approximate relation for estimation of this impeller's design-point efficiency is:

$$\eta = 0.80 - 1.5 \times 10^{-7} \times N \text{ (rpm)} \quad (3)$$

In spite of the uncertainties in such a relation, the decrease in efficiency with increase in speed is a trend for this compressor impeller that relates to the increased sensitivity of the flow to compressibility effects at the higher speeds.

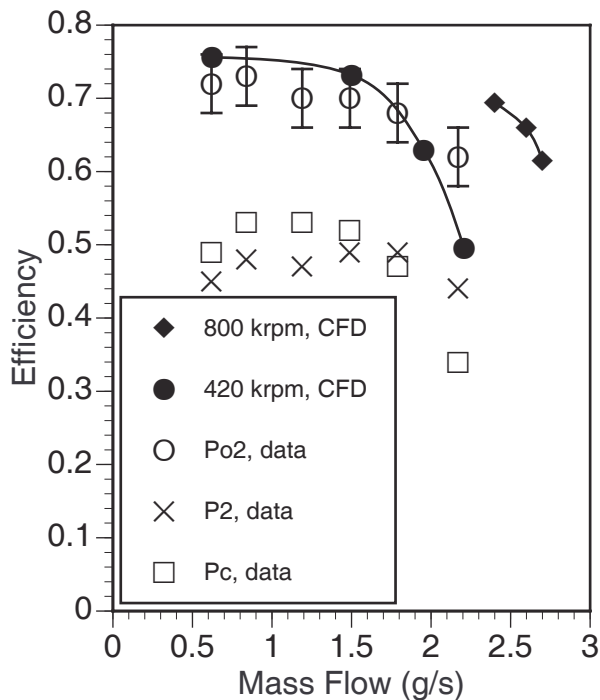


Figure 6 Adiabatic efficiency based on three different pressures.

Effects of rotor blade clearance

In the final phase of the program an attempt was made to evaluate the effects of reduction of axial clearance from the original experimental value of 200 μm (20 % of tip-region blade span, b_{tip}). Additional experiments were conducted at 420 krpm for two smaller clearances 150 μm and 100 μm , the clearance used in the original CFD analysis. Unfortunately, at 100 μm a catastrophic bearing failure occurred after only two, high flow rate data points were obtained so these data were not useful. This event also terminated the experimental program.

A small increase in efficiency of about 0.02 points at DPS appeared in the data when clearance was lowered from 200 μm to 150 μm . It was concluded that this trend could be examined by further use of CFD alone. The original CFD employed a 100 μm clearance, and the new CFD studies were conducted at 200 μm and at a clearance of 50 μm clearance.

The results of all five cases are compared in Figure 7 (work input coefficient), Figure 8 (pressure ratio), and Figure 9 (adiabatic efficiency). Solid curves connect the computed points. The experimental data is shown using open symbols without the addition to vertical bars to represent experimental uncertainty which may be read from Table 2.

The cases in these figures are identified in the legends to indicate the clearance, e.g. CFD/50 means that the clearance is 50 μm , and uniform along the whole blade from inducer inlet to the tip of the blade at the rotor exit plane. In the two experimental cases, the key to the results is different because clearance was varied by moving the rotor axially not by "removing" a fixed portion of the blade span as for the three CFD cases. For example, DATA/200-tip means that the axial clearance between blade tip and shroud wall is 200 μm only at the rotor tip. However, because of the bend from axial- to radial-flow, clearance decreases along the blades, from the designated value at the rotor tip down to the inducer leading edges.

These dissimilarities in geometry are one possible reason why the CFD results at 200 μm don't agree with the experiments at 200 μm (tip), but they seem to align better with the CFD at 100 μm . It is possible that smaller clearance in the inducer portion of the blades is as important as axial clearance at the rotor tip. However, until more data becomes available, the best that can be

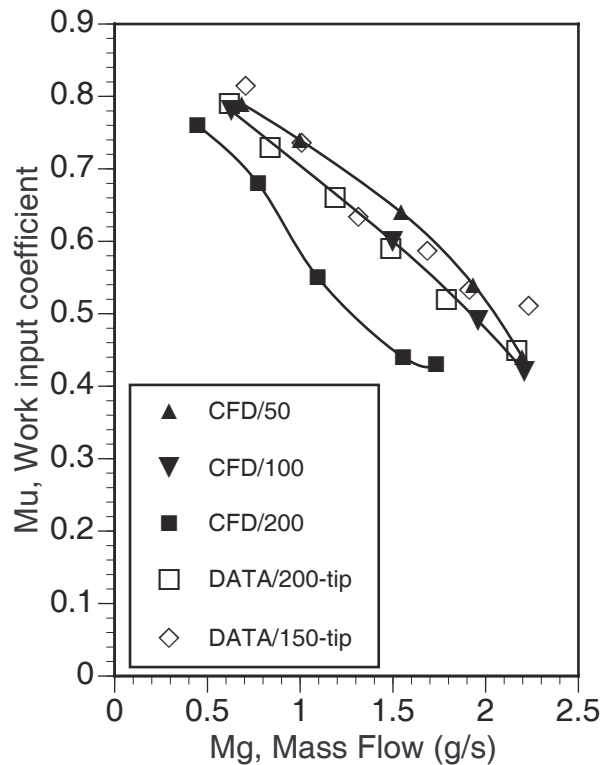


Figure 7 Effects of clearance on work input coefficient

said is that both methods are in general agreement in regards the trends of the effect.

Taken alone, the three curves representing the CFD results show that clearance has important effects on performance. Clearances seen here (20% to 5% of b_{tip}) are large compared to those generally encountered in the study of clearance effects for normal, large-scale radial flow compressors (Senoo and Ishida, 1987), and the effects of change of clearance are also significant. For example, near DPS (1.25 g/s) work input, Fig. 7, and efficiency, Fig. 9, both increase by about 0.1 points for every 100 μm (10% of b_{tip}) of decrease in gap between blade ends and shroud wall.

CONCLUSIONS

A micro-scale (12 mm in diameter), silicon-nitride rotor (turbine-compressor-shaft), has been built, and the performance of the radial-flow compressor impeller has been determined by experiment up to speeds of 420 krpm. Performance was also obtained by CFD and at 420 krpm, and at the design speed, 800 krpm. In addition, CFD was carried out for three different blade-to-shroud clearances, and results compared to experimental data at two clearances.

The relatively good match of experimental and the CFD results at 420 krpm suggests that current, preliminary design methods adapted to low Reynolds number conditions, when combined with CFD techniques, can be used to develop rotors for a micro-scale, gas-turbine engine with fully three-dimensional turbine and compressor impellers. CFD, in this case, proved very useful in determination of the effects of the large blade-to-shroud clearances on the performance of the impeller. However, tests confirming predicted performance at full operating speed, 800 krpm, are still to be obtained.

With the ultimate development of high-speed bearing technology, and the application of Mold SDM process for manufacture of the hot rotating elements in silicon nitride, a fist-sized micro gas-turbine engine appears to be a possibility.

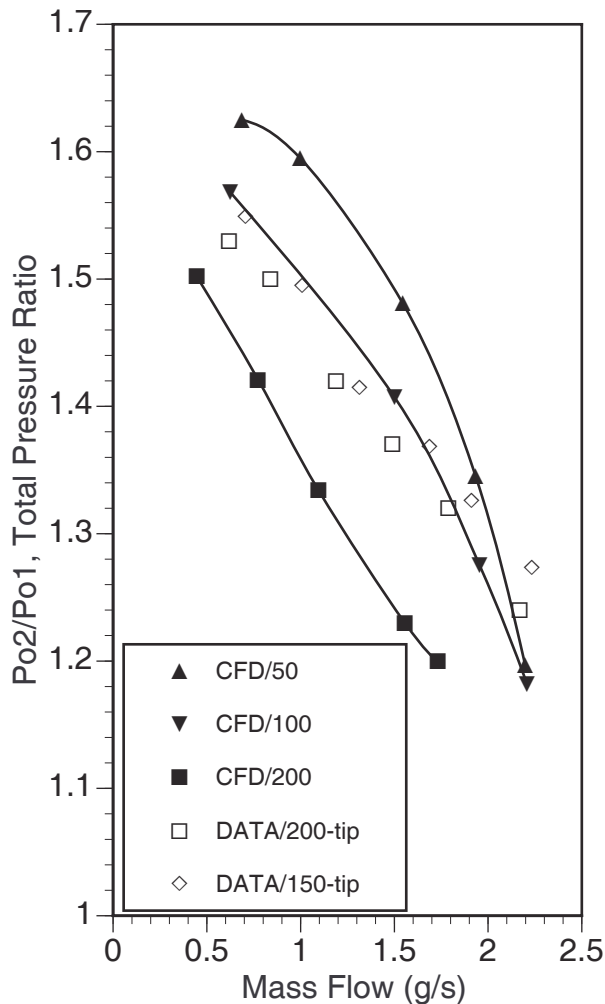


Figure 8 Effects of clearance on pressure ratio

ACKNOWLEDGEMENTS

We recognize Frank Holman and his team at M-Dot Aerospace, Inc. for contributions to the preliminary design. The contributions of Tibor Fabian, Tom Hasler and Bernard Liu of the Rapid Prototyping laboratory at Stanford University in test rig design, assembly and rotor sintering are gratefully acknowledged. The support for ceramic processing by Atsushi Koizumi of Honda R&D Co., Ltd. is also greatly appreciated. We also thank Mineyasu Oana for carrying out the CFD computations. Finally, we thank Prof. Robert Moffat of Stanford for his analysis and suggested solution for the temperature measurement problem.

REFERENCES

Arima, T., Sonoda, T., Shirotori, M., Tamura, A., and Kikuchi, K., 1999, "A numerical investigation of transonic axial compressor rotor flow using a low-Reynolds-number $k-\epsilon$ turbulence model," *ASME Journal of Engineering for Gas Turbines and Power*, 121: pp. 45-58.

Casey, M.V., 1985, "The effects of Reynolds number on the efficiency of centrifugal compressor stages," *ASME Journal of Engineering for Gas Turbines and Power*, 107: pp. 541-548.

Cooper, A.G., Kang, S., Kietzman, J.W., Prinz, F.B., Lombardi, J.L., and Weiss, L.E., 1999, "Automated Fabrication of Complex Molded Parts Using Mold Shape Deposition Manufacturing," *Materials and Design*, 20(2/3): pp. 83-89.

Epstein, A.H., Jacobson, S.A., Protz, J.M., and Fréchette, L.G., 2000, "Shirtbutton-sized gas turbines: the engineering challenges of micro high speed rotating machinery," *Proceedings, 8th Int'l Symposium on Transport Phenomena and Dynamics of Rotating Machinery*, Honolulu, Hawaii.

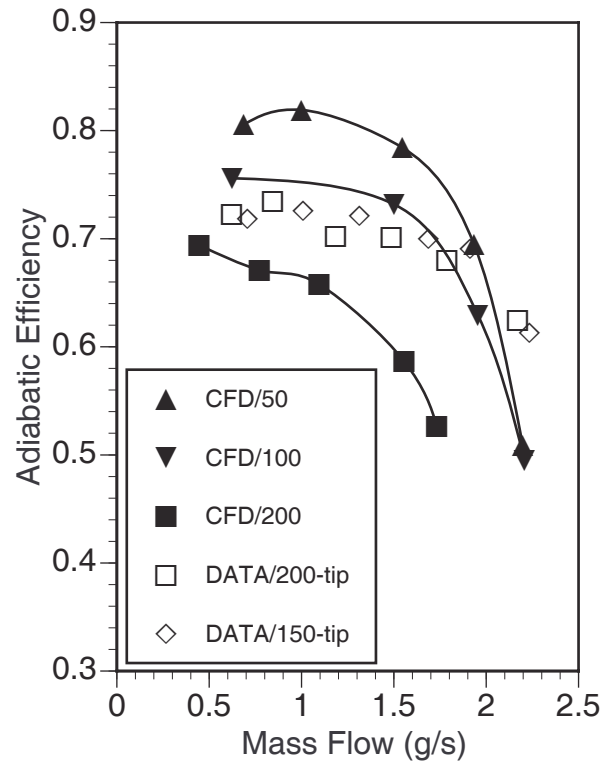


Figure 9 Effects of clearance on adiabatic efficiency

Isomura, K., and Tanaka, S., 2002, "Design of a Micromachined Gas Turbine with 3-Dimensional Impeller," *Proceedings, The 9th of International Symposium on Transport Phenomena and Dynamics of Rotating Machinery*, Honolulu, Hawaii.

Jacobson, S.A., 1998, "Aerothermal challenges in the design of a microfabricated gas turbine engine," *Proceedings, 29th AIAA fluid Dynamics Conference*, Albuquerque, NM.

Kang, S., 2002, "Fabrication of ceramic components for a micro gas turbine engine", Ph. D. thesis, Stanford University, Stanford, CA

Kang, S., Johnston, J.P., Arima, T., Matsunaga, M., Tsuru, H., and Prinz, F.B., 2003, "Micro-Scale Radial-Flow Compressor Impeller made of Silicon Nitride - Manufacturing and Performance," Paper No. GT2003-38933, *ASME Turbo Expo 2003*, Atlanta, Georgia, USA, June 16-19, 2003.

Kline, S.J. and McClintock, F., 1953, "Describing uncertainties in single sample experiments," *Mechanical Engineering*, ASME, pp. 3-8.

Senoo, Y., and Ishida, M., 1987, "Deterioration of Compressor Performance Due to Tip Clearance of Centrifugal Impellers," *J. of Turbomachinery*, Vol. 109, pp. 55-61.

Stampfl, J., Liu, H-C, Nam, S.W., Sakamoto, K., Tsuru, H., and Kang, S., 2002, "Rapid Prototyping and manufacturing by gelcasting of metallic and ceramic slurries," *Materials Science and Engineering A*, 334: pp. 187-192.

Wachtman, J.B., 1996, "Mechanical Properties of Ceramics," 1996, New York: John Wiley & Sons, Inc.